Express Polymer Letters Vol.18, No.3 (2024) 337–347
Available online at www.expresspolymlett.com
https://doi.org/10.3144/expresspolymlett.2024.24

Research article

Tradeoff in interfacial shear strength and elastic properties in functionalized graphene oxide nanocomposites

Hashim Al Mahmud[1,2*], *Sagar Umesh Patil*[2], *Gregory Odegard*[2]

[1]Department of Mechanical Engineering, University of Kufa, P.O. Box 21, 54001 Kufa, Najaf Governorate, Iraq
[2]Department of Mechanical Engineering-Engineering Mechanics, Michigan Technological University, 1400 Townsend Drive, MI-49931 Houghton, USA

Received 20 October 2023; accepted in revised form 9 December 2023

Abstract. Graphene oxide (GO) nanoplatelets can be used to reinforce neat resin or the matrix phase of fiber composites for improved mechanical properties. Although the oxygen content levels in GO and reduced graphene oxide (rGO) strongly influence the interface with the polymer, experimental-based optimization of the oxygen content for enhanced composite properties is difficult and time-consuming. Fortunately, molecular dynamics (MD) simulation can be used to efficiently predict the interfacial properties of composite on the molecular level and provide physical insight into the effect of the oxygen content of rGO. In this study, MD is used to predict the elastic properties of rGO/epoxy interfaces and the corresponding interfacial shear strength (IFSS) for different oxygen content levels. The results indicate that increasing levels of oxygen in rGO results in interfaces with a reduced in-plane elastic modulus but a substantially higher IFSS. These results are important for the design of rGO/epoxy composites for specific engineering applications.

Keywords: *mechanical properties, reinforcement, morphology, interfacial interaction, waviness, wrinkling*

1. Introduction

Polymer matrix composites (PMCs) based on carbon nanostructure reinforcement have the potential to be used in aerospace structures with demanding mechanical requirements. Specifically, graphene oxide (GO) and reduced graphene oxide (rGO) [1] reinforcements can boost the properties of traditional carbon-fiber reinforced PMCs, thus expanding their applications in sensors, electronics, and energy storage devices. Although rGO reinforcement is a key approach to improving the bulk properties of PMCs [2–7], the synthesis of rGO morphology using the well-known chemical or thermal approaches [8, 9] and probing its interplay with polymer matrices is still complicated. In other words, experimental investigation of the interphase between the polymer and rGO is a time-consuming and expensive process. Computational tools such as molecular dynamics (MD) can provide physical insights into these interfaces by analyzing the molecular structure and interactions occurring between the rGO and polymer molecules at the interface and predict the interfacial mechanical behavior [10, 11]. As a result, such computational approaches can be integrated with experimental observations to acquire rigorous interpretation of the possible change in the material behavior and its engineering characteristics.

Previously, the authors have demonstrated that a multi-scale framework consisting of MD and micromechanics can be effectively utilized to predict the effective properties of hybrid nanocomposites [12–16]. A reactive force field was used for all these MD simulations. They predicted effective mechanical properties of carbon fiber (CF)/graphene nanoplatelets (GNP)/epoxy hybrid composites and provided evidence of re-orientation of phenyl rings in the epoxy

*Corresponding author, e-mail: hashimn.almahmood@uokufa.edu.iq

molecules near the GNP surface [12]. They further studied the effect of highly concentrated GO and functionalized GNPs [14] on the mechanical properties of hybrid nanocomposites. They further extended their work to study the effect of GNP and CF volume fractions, GNP aspect ratio, and laminate lay-ups on the bulk level mechanical properties of hybrid nanocomposites [15]. The results presented in all these studies agree well with experimental data in the literature. Even though these studies provide an experimentally validated multi-scale framework for simulating functionalized hybrid nanocomposites, they do not fully address the influence of varying oxygen content (of GNP-based reinforcement) on the overall mechanical behavior. Such information is important for the design of hybrid PMCs with optimal mechanical properties.

In this work, MD simulation is used to study the effect of varying carbon-to-oxygen ratio (C:O) of the GNP in rGO functionalization on the interfacial interaction energy (*IIE*), elastic properties, and interfacial shear strength (*IFSS*) of rGO/epoxy nanocomposites. A reactive force field was used to model three different C:O molar ratios: 10, 20, and 40. These C:O ratios were considered to model the possible oxygen level in rGO, considering the span from a very low oxygen level in GNP to highly concentrated graphene oxide in GO. The results show that the C:O concentration significantly influences the properties of the nanocomposite, and a tradeoff between the *IFSS* and the elastic properties is discussed. These results along with those of previous studies [12–15, 17], can be used as design guidelines to fabricate hybrid nanocomposites tailored for specific applications.

2. Computational modeling

2.1. Material system

An epoxy system consisting of a di-functional diglycidyl ether bisphenol A (DGEBA) resin commercially available as EPON828 and a tetra-functional aromatic hardener diethyl toluene diamine (DETDA) commercially available as EPIKURE W curing agent was modeled in this work. Both of the resin and the hardener are modeled based on the reported data provided by HEXION Specialty Chemicals, Inc. PO Box 4500, located in Houston, TX 77210-4500, USA. As per HEXION, typical applications using Cured EPON828 systems exhibit tensile values surpassing 69 MPa, along with modulus values exceeding 2750 MPa, indicating high strength and rigidity. For applications requiring high flexibility, formulations can be adjusted to achieve up to 300% elongation.

The reinforcement of the considered nanocomposite is graphene oxide (GO) and reduced graphene oxide (rGO) nanoplatelets, which are modeled based on the reported data provided by Graphene America, located in Charlotte, North Carolina, USA. It has been reported that Young's modulus of GO/rGO is in the range of 380–470 GPa, depending on the oxygen content [18]. The lower the oxygen content, the higher the value of Young's modulus is obtained. Similarly, increasing oxygen content was found to cause a decrease in both the intrinsic strength (47.8–38.6 GPa) and critical failure strain (20–16%). Furthermore, the wrinkled structure of GO nanoplatelets was found to be increased with increasing oxygen content, and thus, a degradation in their mechanical properties has been observed.

Figure 1 shows the skeletal and MD structures of both epoxy components in addition to a representative rGO MD sample. The LAMMPS MD modeling software package was implemented to perform all simulations in this work [19].

2.2. MD simulation details

Both monomers shown in Figure 1 were initially modeled using the OPLS-All Atom fixed-bond force field [20]. The DGEBA and DETDA monomers were mixed in a stoichiometric molar ratio of 2:1, constituting a total of 6192 atoms. The monomers were then combined with rGO layers with varying C:O ratios to create layered models as shown in Figure 2. Individual MD models were built for each C:O molar ratio, that is, 10:1, 20:1, and 40:1 (henceforth referred to as 10, 20, 40, respectively) and compared

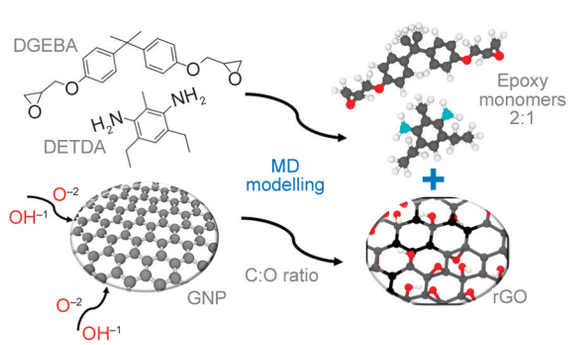

Figure 1. Skeletal and MD structures of DGEBA resin, DETDA hardener, and rGO MD sample. C:O ratio refers to the ratio of the number of graphitic carbon atoms to functionalizing oxygen atoms.

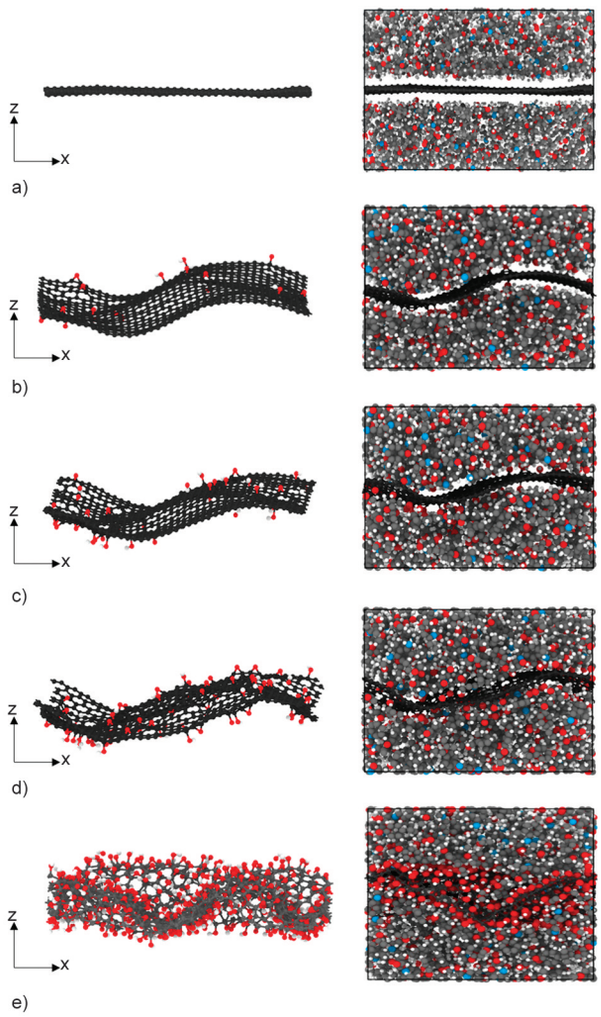

Figure 2. MD models of rGO/epoxy nanocomposites with C:O ratios of a) ∞, b) 40, c) 20, d) 10, and e) 1.5. The carbon (sp^2) atoms are represented as black, carbon (sp^3) as gray, hydrogen as white, nitrogen as blue, and oxygen as red.

with the properties of pristine (C:O ratio = ∞; no oxygen functionalization) and highly concentrated (C:O ratio = 1.5:1, henceforth referred to as 1.5) GO nanocomposites from the literature [14]. The rGO layers for varying C:O ratios were created by functionalizing pristine GNP layers consisting of 836 C atoms with varying numbers of hydroxyl (–OH) groups and oxygen (O) atoms. Table 1 shows the details of the MD models for all cases. Henceforth, the five cases will be refereed by the corresponding C:O ratio. The combined MD models were then densified and equilibrated as described elsewhere [12, 14, 15]. Periodic boundary conditions were used for all simulations.

It is important to note that GO40/epoxy, GO20/epoxy, and GO10/epoxy were established based on the validated MD models (GNP/epoxy and GO1.5/epoxy) indicated in Table 1. In addition, the specified simulation box dimensions were established to account for the limitations in computational resources, especially for MD simulations with ReaxFF force field. Despite the number of atoms in the epoxy system (6192 atoms) and GNP (836) were kept constant in all MD models, there is a relative change in the simulation box dimensions, which can be attributed to the change in oxygen functional group content (*i.e.*, C:O ratio) attached to the GNP. These oxygen functional groups change the morphology of the nanoplatelets and produce relative differences in their waviness factors (*WF*). Thus, the lateral dimensions (along x and y) of the simulation box decrease as it is governed by the nanoplatelet size. This, in turn, produces an increase in the length of the simulation box along the z direction.

After equilibration, the crosslinking between the reactive epoxide groups in DGEBA and reactive amine groups in DETDA was performed in the presence of the rGO layers using the 'fix bond/create' command in LAMMPS [12]. An average crosslinking density of 80% was achieved, where the crosslinking density is defined as the ratio of the actual number of covalent bonds formed between the resin and hardener monomers to the maximum number of covalent bonds that could be formed. After crosslinking, the MD models were transitioned from the OPLS force field to a reactive force field (ReaxFF) using the Liu *et al*. [21] parameter set to simulate bond scission

Table 1. MD model details for various C:O ratios.

Cases	C:O ratio	No. of functionalized atoms (–OH and =O)	Total no. of atoms	Simulation box size approximated to the nearest tenth [Å]	The waviness factor of the nanoplatelet
GNP/epoxy[a]	∞	0	7028	47.6×47.7×29.7	1.000
rGO40/epoxy	40	32	7060	47.2×47.7×30.5	0.982
rGO20/epoxy	20	63	7091	47.3×47.6×30.3	0.988
rGO10/epoxy	10	126	7154	46.9×47.5×31.2	0.967
GO1.5/epoxy[a]	1.5	813	7841	42.4×43.4×38.4	0.903

[a]data of GNP/epoxy and GO1.5/epoxy were taken from [14]

and non-linear bond deformation. The interfacial interaction energy (*IIE*), elastic properties, and waviness factor (*WF*, measured as the ratio between the actual 'wrinkled' length to the flat length) were predicted using methods comprehensively described previously [12, 14, 15] and are briefly described below for completeness.

The *IIE* between the nanoplatelets and epoxy was calculated by subtracting the individual potential energies of epoxy and GNP from the total potential energy of the entire system using the constant pressure and temperature (NPT) ensemble, simulated with 0.1 fs timesteps for 1 ns at 300 K and 1 atm pressure. It is important to note that the use ReaxFF force field in the current MD simulations helps to efficiently evaluate and predict the mutual *IIE* between constituents in such nanocomposites [13, 22]. This is attributed to its accounting for long-range non-covalent interactions.

To predict elastic properties, all 5 MD replicates for each C:O ratio were subjected to tensile and shear deformation simulations at 0.1 fs timesteps for a total of 0.5 ns at a strain rate of $1 \cdot 10^8$ s^{-1} at 300 K and 1 atm pressure using the Nose/Hoover thermostat and barostat. The NPT and NVT (constant volume and temperature) ensembles were used to carry out tensile and shear simulations, respectively. Tensile deformations were simulated in the x- and y-directions to predict the in-plane elastic modulus ($E_{ip} = (E_{xx} + E_{yy})/2$) and in-plane Poisson's ratio ($\nu_{ip} = (\nu_{xy} + \nu_{yx})/2$), and in the z-direction to predict the out-of-plane elastic modulus ($E_{op} = E_{zz}$) and out-of-plane Poisson's ratio ($\nu_{op} = (\nu_{zx} + \nu_{zy})/2$). The shear deformations were simulated in the xy-plane to predict the in-plane shear modulus ($G_{ip} = G_{xy}$) and in the xz- and yz-planes to predict the out-of-plane shear modulus ($G_{op} = (G_{xz} + G_{yz})/2$).

For the prediction of *IFSS*, pull-out simulations were performed with MD simulation using a similar approach described elsewhere [23–25]. Figure 3 shows a representative image showing the zigzag and armchair directions in graphitic structure and a MD model set up for the pull-out simulations. Periodic boundary conditions were used in all three directions of the simulation cell; the fixed boundary condition in Figure 3b is shown just for illustration purposes. A pulling force was applied at each carbon atom in the GNP and the epoxy matrix was fixed by a spring force in the opposite direction to the pulling force. The displacement of the epoxy layer fluctuated around 0 Å as the atoms in the nanoplatelet were pulled. A spring constant of 1000 (kcal/(mol·Å))/Å was used in these simulations. The GNP layer was pulled along both zigzag and armchair directions as shown in Figure 3a. To capture the relative separation onset of the GNP from the epoxy matrix, the pulling force was gradually increased from zero to a maximum value. Small increments ($5 \cdot 10^{-11}$ kcal/(mol·Å) for C:O = ∞ and $0.125 \cdot 10^{-4}$ kcal/(mol·Å) for all other C:O ratios) of pulling force enabled the monitoring of the relative slipping between the polymer and nanoplatelet. The maximum pulling force value was determined by running a preliminary MD pull-out simulation that allowed for the complete separation of polymer and nanoplatelet. For C:O = ∞, the pull-out simulation was run for 1 ns with a time-step of 0.1 fs, and the maximum force was $5 \cdot 10^{-4}$ kcal/(mol·Å). Whereas for all other C:O ratios, the pull-out simulation was run for 0.5 ns with a time-step of 0.25 fs with a maximum pulling force of 0.25 kcal/(mol·Å). The *IFSS* was estimated by averaging the pulling force values over a window starting just before ~5 Å of nanoplatelet displacement and over all pulling force values

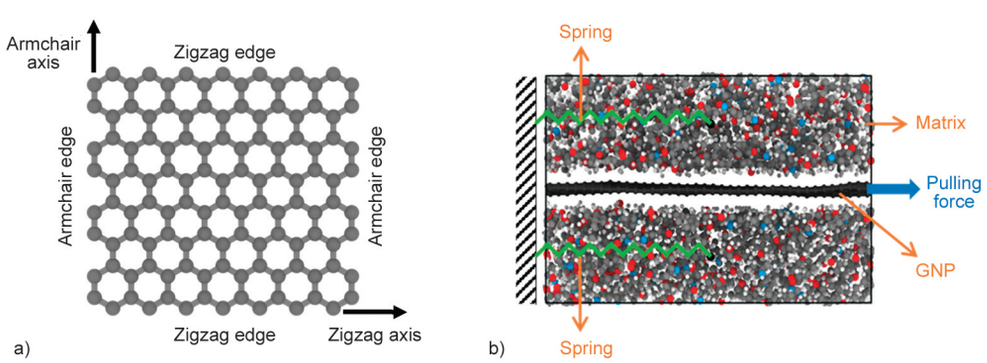

Figure 3. Representative image showing a) the armchair and zigzag axes and b) pull-out simulation set-up with the applied pulling force and reaction springs.

over the steady state slipping behavior of the nanoplatelet. The averaged pulling force value was multiplied by the total number of carbon atoms in the graphene lattice for each case to obtain the overall *IFSS* [13].

3. Results

This section describes the results of the MD simulations to predict *IIE*, elastic properties, and *IFSS* for three C:O ratios in rGO/epoxy composites. The results are compared with pristine (C:O = ∞) GNP/epoxy and highly concentrated (C:O = 1.5) GO/epoxy nanocomposite taken from the literature [14]. The value in the plots for each C:O ratio is the average of five replicates and the error bar represents the standard deviation associated with the replicates.

3.1. Interfacial interaction energy (*IIE*)

Figure 4 shows the *IIE* for each C:O ratio of graphene nanoplatelets with the epoxy matrix at the interface. For the data in Figure 4, the values are all negative, and larger magnitudes of negative values indicate improved and more favorable *IIE*. *IIE* is calculated considering different energy terms. Some of these energy terms are positive and represent the repulsive portion in *IIE*. However, the negative energy terms represent the attractive portion in *IIE*. Due to the affinity between the constituents in such nanocomposites, the attractive portion in the *IIE* surpasses the repulsive portion and produces an overall negative *IIE*. This, in turn, improves the interfacial non-covalent binding, which is more favorable for better load transfer at the interface. It is important to note that the increase in the standard deviation levels observed for the predicted *IIE* in rGO/epoxy and GO/epoxy relative to GNP/epoxy MD models can be attributed to the increased waviness value in rGO and GO.

The *IIE* is least favorable for the C:O = ∞ as compared to other cases. The *IIE* improves with decreasing C:O ratios from 40 to 1.5. The improvement in the *IIE* can be attributed to the addition of oxygen functional groups on the GNP surface with decreasing C:O ratio. It has been previously established that the improvement in the *IIE* was attributed to the tremendous evolution in Coulomb energy term at the interface in addition to the interfacial covalent and H-bond between GO and epoxy matrix [13]. This occurs at the expense of the relatively weaker π-π conjugation and interfacial van der Waals energy terms, which dominate the *IIE* at the interface between GNP and

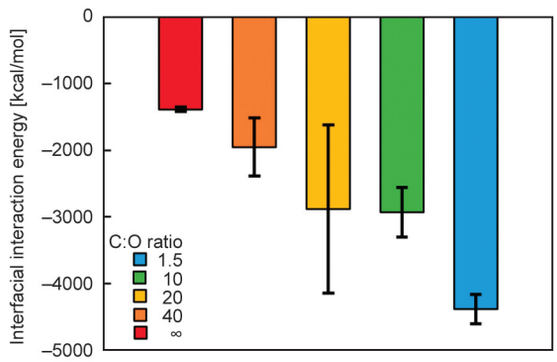

Figure 4. Interfacial interaction energy (*IIE*) as a function of C:O ratio in rGO/epoxy nanocomposite.

epoxy matrix. The loss in these two energy terms can be attributed to the induced waviness in rGO and GO structures, which produces a misalignment between carbon rings in the nanoplatelet hexagonal structure and phenyl rings in the epoxy molecules [12]. Generally, energy evolution and the produced increment in the *IIE* seem to be directly proportional to the amount of oxygen functional groups (*i.e.*, inversely proportional to the C:O ratio).

The waviness in the GNPs is induced as a result of the addition of oxygen atoms to the GNP surface. The waviness factor (*WF*) is a measure of the wrinkling degree of the graphene nanoplatelet, as shown in Table 1 for all the cases investigated herein. A flat nanoplatelet surface is defined as *WF* = 1. The *WF* decreases with increasing wrinkling of the nanoplatelets. Thus, as shown in Table 1, GNP with C:O = ∞ maintains a flat surface with the highest *WF* of 1. The *WF* decreases with decreasing C:O ratio and increasing concentration of oxygen atoms on the GNP surface, which produces a more wrinkled and rougher surface of the nanoplatelet. Despite the above-mentioned negative role of waviness on *IIE* (interfacial rings-misalignment), the waviness of graphene nanoplatelets could concurrently have positive effects on improving *IIE*. This could substitute and even significantly outmost the loss in the *IIE*, yet it is difficult to quantify. As shown in Figure 5, the addition of oxygen atoms on the GNP surface changes the profile of spatial mass density distribution at the interphase region. Clearly, the GNP waviness structure disperses the mass density concentration at the center (*i.e.*, reduces the magnitude of the mass density spike caused by a flattened GNP). This reduction substitutes and fills the GNP-epoxy interfacial gaps with zero mass density (Figure 5a) and produces a favorable entangled interface between the two constituents

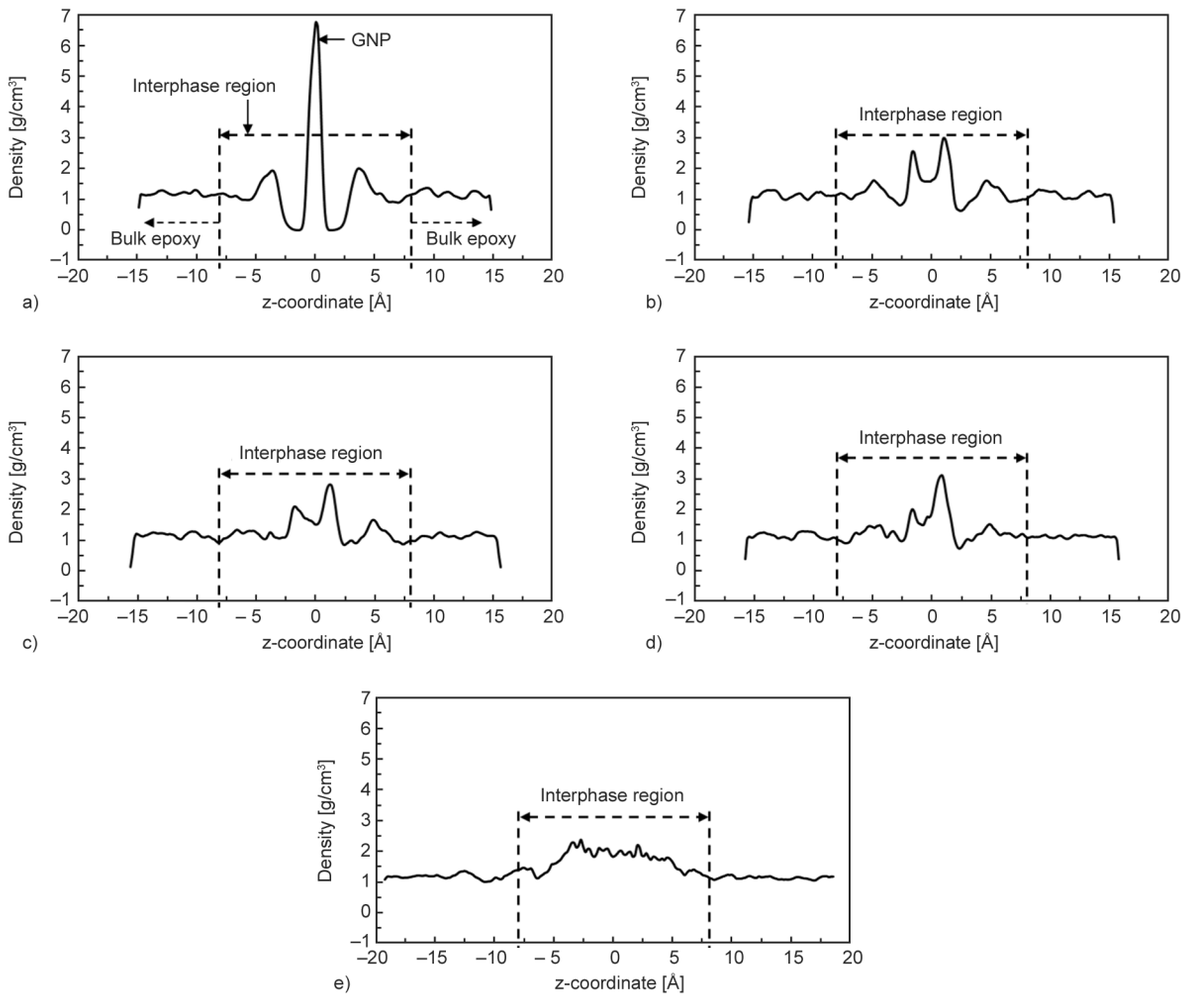

Figure 5. Density profiles of rGO/epoxy nanocomposite with C:O ratio a) ∞, b) 40, c) 20, d) 10, and e) 1.5.

(Figure 5b–5e). The interfacial entanglement seems to be improved and directly proportional to the functionalization degree with oxygen groups (*i.e.*, inversely proportional to the C:O ratio). This change in morphology and the promoted interfacial entanglement at the interphase could be accounted for by the increase in the *IIE*. The role of wrinkled graphene nanoplatelets and functional groups in improving the interfacial interaction and the integrity of polymer-based nanocomposites can be found elsewhere [6, 7, 26–30].

3.2. Elastic properties

Figure 6 shows the in-plane and out-of-plane elastic moduli, Poison's ratios, and shear moduli for all C:O ratios. Figure 6a shows that the highest E_{ip} value of 127.5 GPa is predicted for C:O = ∞ and the lowest value of 13.7 GPa for C:O = 1.5 [14]. This is mainly attributed to the strong bonds between sp^2 carbon atoms and the pristine and flat hexagonal GNP structure for C:O = ∞ as compared to other C:O ratios as shown in Figure 2. The reinforcing efficiency of GNP is highly sensitive to the GNP molecular structure. Attaching oxygen functional groups to the sp^2 carbon atoms in the GNP will change the hybridization to the sp^3 type, which consequently weakens the bonding between the other bonded carbon atoms. The random distribution of oxygen groups on the GNP surface creates a hybrid network of C–C bonding with a mix of strong sp^2–sp^2, weaker sp^2–sp^3, and largely weaker sp^3–sp^3 bonds. Such a hybrid bond structure produces a wrinkled GNP structure. Therefore, the E_{ip} is the lowest for C:O = 1.5 as most of the carbon atoms have sp^3 hybridization. The waviness factor (*WF*) also decreases with decreasing C:O ratio. The highly wrinkled structure (*WF* = 0.903) for C:O = 1.5 produces C–C bonds that are not aligned in the x-y direction and thus do not strongly reinforce in the x-y direction. In addition, the unbalanced strength between C–C bonds caused by the arbitrary distribution of oxygen groups produces an early confused and weak reinforcing response. This delays the reinforcing

effect of the nanoplatelet under tensile loading until it becomes straight, which is most likely to occur at high strain values. Even though this is an intuitive behavior, it is quite complicated to quantify the wrinkling effect on the nanoplatelet reinforcing value. This is because wrinkling concurrently helps to support the interlocking mechanism between the epoxy matrix and nanoplatelet which is accounted for improving the reinforcing effect of the nanoplatelet.

Figure 6b shows that the C:O = ∞ case registers the highest reinforcing effect with a E_{op} value of ~5 GPa, which is greater than the modulus of pure epoxy (2.72 GPa [31]). No significant difference in E_{op} was observed between all other C:O ratios. While E_{ip} of the nanocomposite is dominated by the in-plane elastic modulus of the nanoplatelet, E_{op} is dominated by the elastic modulus of the epoxy system. The slight increase in E_{op} observed for the nanocomposites relative to that in the pure epoxy system can be attributed to the mutual π-π stacking at the interphase region. For GNP/epoxy nanocomposites, it has been demonstrated that the phenyl rings in the epoxy matrix have the tendency to align with the GNP plane, providing a non-covalent interfacial binding between the two constituents [12]. However, the π-π stacking degree seems to be affected by the wrinkled structure of rGO. This produces the fluctuation in the predicted E_{op} observed for different C:O ratios. Figures 6d and 6f shows that the predicted ν_{op} and G_{op} increase with decreasing C:O ratio, which is due to the increase in the bonded network between the GNP surface and functional groups. Figure 6c shows that ν_{ip} decreases with decreasing C:O ratios. This is likely due to the morphology of the nanoplatelet. The C:O = ∞ case

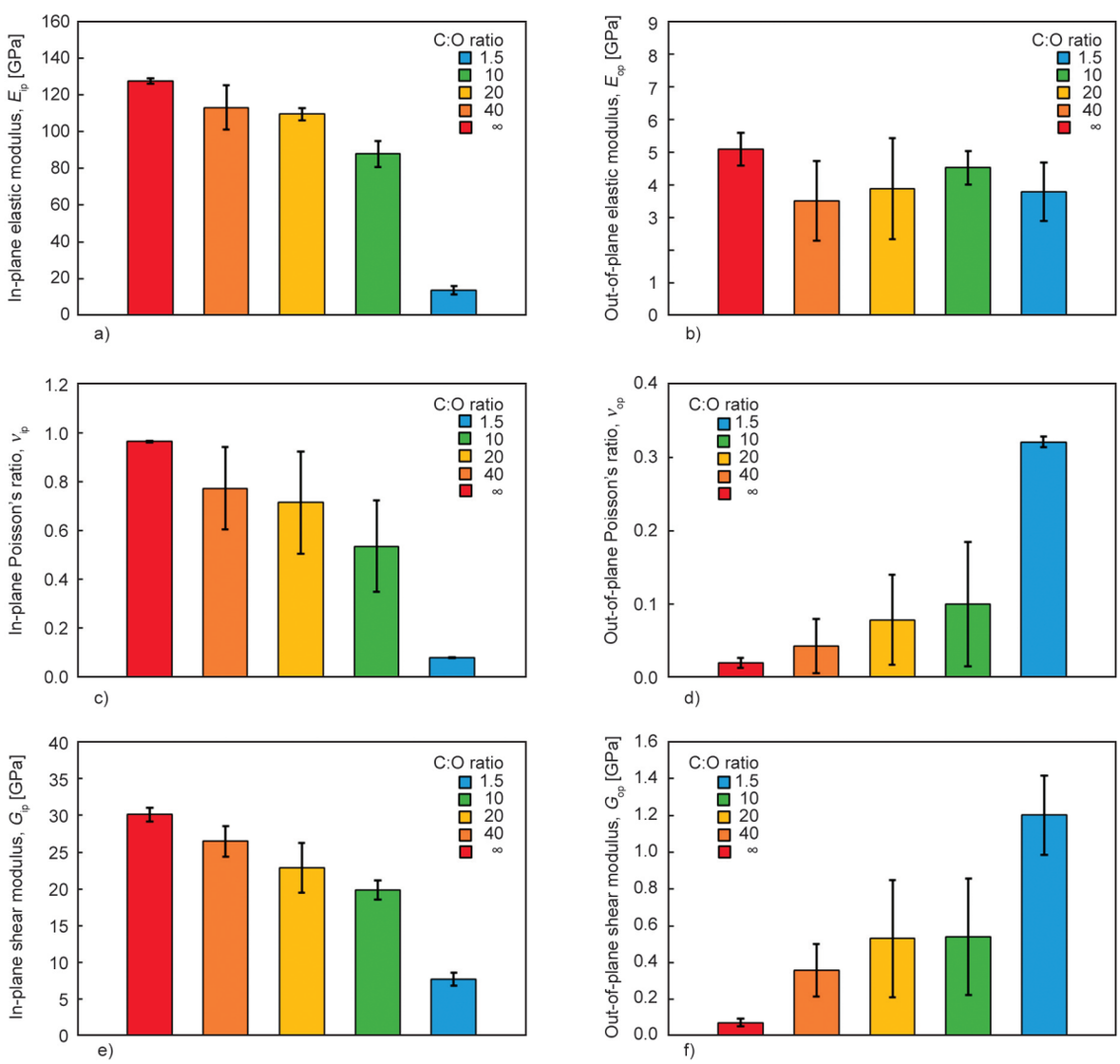

Figure 6. a) In-plane and b) out-of-plane elastic modulus; c) in-plane and d) out-of-plane Poisson's ratio; e) in-plane and f) out-of-plane shear modulus as a function of C:O ratio in rGO/epoxy nanocomposite.

with high *WF* factor (flat) maintains large lateral Poisson's effect and for C:O = 1.5 with lowest *WF* factor of all cases (highly wrinkled) has lower lateral Poisson's effect. Similar to E_{ip} and ν_{ip}, G_{ip} shown in Figure 6e also decreases with decreasing C:O ratios, which can be attributed to the integrity of the nanoplatelet which erodes with decreasing C:O ratio.

3.3. Interfacial shear strength (*IFSS*)

Table 2 shows the *IFSS* averaged over the five MD replicates along the two axes for all C:O ratios. Figure 7 shows the plots of displacement of graphene nanoplatelets as a function of pulling force along the zigzag and armchair axes.

Table 2 and Figure 7 show that the *IFSS* and the pulling force respectively increases significantly as soon as oxygen atoms were added to the GNP surface by comparing the predicted *IFSS* for C:O = ∞ with other cases. For all C:O ratios, the *IFSS* registers the highest value of 250.88 kcal/(mol·Å) for C:O = 1.5 and the lowest value of 0.40 kcal/(mol·Å) for C:O = ∞. The *IFSS* increases with decreasing C:O ratio because the addition of oxygen atoms to the GNP surface increases its surface roughness, which then increases the interactions between oxygen atoms and epoxy molecules (Figure 4). Therefore, more pulling force is required to pull the GNP layer relative to the epoxy matrix. Figure 7 shows that for C:O = ∞, there is a clear difference in the force-displacement response of GNP when pulled along the zigzag and armchair axes. This difference can be attributed to the different energy-well landscapes along the two axes [13]. In addition, for C:O = ∞, the *IFSS* for both zigzag and armchair axes is the lowest as compared to all other C:O ratios. This is likely because of the absence of functional groups on the GNP surface, which makes the GNP slide easily with minimum pulling force relative to the epoxy matrix. Figure 8 shows normalized values of E_{ip} and *IFSS* for increasing levels of C:O ratios. For clarity in the tradeoff effect plotted between two different metrics, both E_{ip} and *IFSS* values were normalized by the corresponding maximum value for each, and C:O ratio values were plotted using a logarithmic scale. For C:O = ∞, E_{ip} of GNP/epoxy registers its highest value, yet there is very weak *IFSS* between GNP and epoxy. For decreasing C:O ratios between 40 and 20, E_{ip} begins to decrease whereas *IFSS* starts increasing. For further decreases of the C:O ratio to 1.5, E_{ip} significantly decreases while *IFSS* reaches its highest value. The data in Figure 8 indicates that compromises in E_{ip} and *IFSS* can be achieved for C:O ratios between 1.5 and 20.

Table 2. *IFSS* [kcal/mole-Å] for various C:O ratios, replicates, and loading directions.

C:O ratio	∞		40.00		20.00		10.00		1.50	
MD replicant	zigzag	armchair	zigzag	armchair	zigzag	armchair	zigzag	armchair	zigzag	armchair
1	0.568	0.538	34.22	41.38	61.55	54.24	98.18	77.49	230.74	259.16
2	0.372	0.333	43.16	40.08	44.83	43.32	104.66	119.70	235.75	246.62
3	0.372	0.345	35.11	33.13	48.33	57.68	111.82	125.24	266.68	224.88
4	0.369	0.343	29.52	17.56	90.60	77.12	94.73	105.65	240.77	261.67
5	0.365	0.395	42.37	37.31	66.46	62.07	97.76	96.14	283.40	259.16
Average	**0.40**		**35.38**		**60.62**		**103.14**		**250.88**	
Standard deviation	**0.08**		**7.67**		**14.75**		**13.66**		**18.23**	

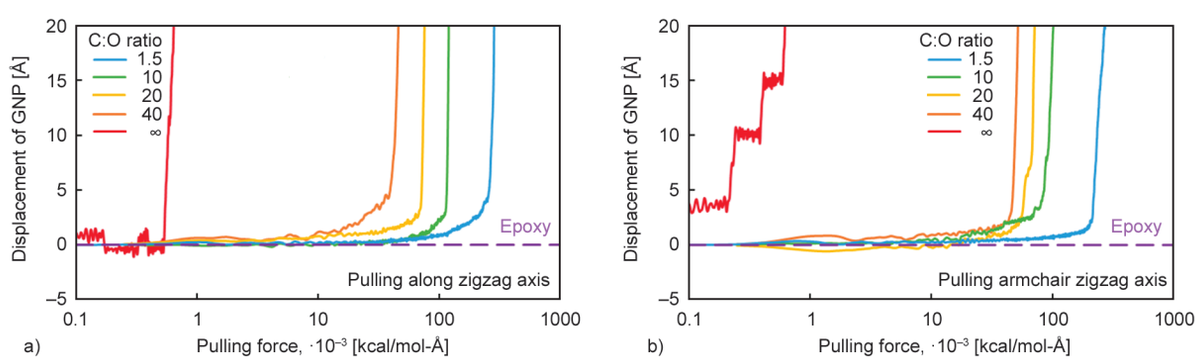

Figure 7. Displacement of GNP as a function of pulling force when the atoms in the GNP layers are pulled along the a) zigzag and b) armchair axes.

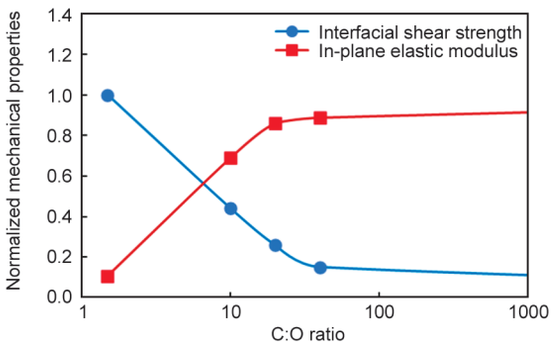

Figure 8. The tradeoff between E_{ip} and *IFSS* caused by varying the C:O ratio (logarithmic scale).

4. Conclusions

The results of this study indicate that decreasing the C:O ratio from ∞ to 1.5 produces a tremendous change in the mechanical properties as follows:

- E_{ip} decreases significantly as the C:O ratio decreases from ∞ to 1.5.
- E_{op} is comparable for all C:O ratios.
- G_{op} and ν_{op} increase significantly as the C:O ratio decreases from ∞ to 1.5.
- The *IIE* and *IFSS* increase significantly as the C:O ratio decreases from ∞ to 1.5.

Based on these results, there is clearly a tradeoff on the decrease in E_{ip} and the increase of *IFSS* over the range of C:O ratios. The tradeoff trend between these two essential mechanical properties has been visually demonstrated. More importantly, the plotted data shown in Figure 8 indicates that compromises in Eip and *IFSS* can be achieved for C:O ratios between 1.5 and 20, with the specific target ratio depending on the engineering application. In other words, the findings presented in this study establish an optimization scheme, which can be adapted to tailor the mechanical properties of rGO/epoxy nanocomposites depending on the C:O ratio. In a broader context, the adopted scheme is crucial for designing nanocomposites as it allows to computationally picture the possible tradeoff in mechanical properties. Considering that computational approaches are cost-effective and time-saving compared to experimental methods. Therefore, this optimization approach can be generalized to be applied to other key processing parameters in polymer-based nanocomposites.

Acknowledgements

This research was partially supported by the NASA Space Technology Research Institute (STRI) for Ultra-Strong Composites by Computational Design (US-COMP) grant NNX17AJ32G. SUPERIOR, a high-performance computing cluster at Michigan Technological University, was used in obtaining the MD simulation results presented in this publication.

References

[1] Kavitha C.: A review on reduced graphene oxide hybrid nano composites and their prominent applications. Materials Today: Proceedings, **49**, 811–816 (2022). https://doi.org/10.1016/j.matpr.2021.05.343

[2] Monteserín C., Blanco M., Aranzabe E., Aranzabe A., Laza J. M., Larrañaga-Varga A., Vilas J. L.: Effects of graphene oxide and chemically-reduced graphene oxide on the dynamic mechanical properties of epoxy amine composites. Polymers, **9**, 449 (2017). https://doi.org/10.3390/polym9090449

[3] Sieradzka M., Fabia J., Biniaś D., Fryczkowski R., Janicki J.: The role of reduced graphene oxide in the suspension polymerization of styrene and its effect on the morphology and thermal properties of the polystyrene/RGO nanocomposites. Polymers, **12**, 1468 (2020). https://doi.org/10.3390/polym12071468

[4] Su Z., Wang H., Tian K., Xu F., Huang W., Tian X.: Simultaneous reduction and surface functionalization of graphene oxide with wrinkled structure by diethylenetriamine (DETA) and their reinforcing effects in the flexible poly(2-ethylhexyl acrylate) (P2EHA) films. Composites Part A: Applied Science and Manufacturing, **84**, 64–75 (2016). https://doi.org/10.1016/j.compositesa.2015.11.033

[5] Bhanuprakash L., Parasuram S., Varghese S.: Experimental investigation on graphene oxides coated carbon fibre/epoxy hybrid composites: Mechanical and electrical properties. Composites Science and Technology, **179**, 134–144 (2019). https://doi.org/10.1016/j.compscitech.2019.04.034

[6] Alipour A., Lin R., Jayaraman K.: Enhancement of performance in flax/epoxy composites by developing interfacial adhesion using graphene oxide. Express Polymer Letters, **17**, 471–486 (2023). https://doi.org/10.3144/expresspolymlett.2023.35

[7] Zhang T., Wang H., Hao Y., Liu C., Zhao Y., Zeng Y.: Optimizing interfacial interactions between functionalized graphene and chitosan for enhanced strength and toughness of composite films. Express Polymer Letters, **17**, 90–103 (2023). https://doi.org/10.3144/expresspolymlett.2023.7

[8] Pei S., Cheng H-M.: The reduction of graphene oxide. Carbon, **50**, 3210–3228 (2012). https://doi.org/10.1016/j.carbon.2011.11.010

[9] Chua C. K., Pumera M.: Chemical reduction of graphene oxide: A synthetic chemistry viewpoint. Chemical Society Reviews, **43**, 291–312 (2014). https://doi.org/10.1039/C3CS60303B

[10] Sun Y., Tang X., Bao H., Yang Z., Ma F.: The effects of hydroxide and epoxide functional groups on the mechanical properties of graphene oxide and its failure mechanism by molecular dynamics simulations. RSC Advances, **10**, 29610–29617 (2020). https://doi.org/10.1039/D0RA04881J

[11] Jang H-K., Kim H-I., Dodge T., Sun P., Zhu H., Nam J-D., Suhr J.: Interfacial shear strength of reduced graphene oxide polymer composites. Carbon, **77**, 390–397 (2014). https://doi.org/10.1016/j.carbon.2014.05.042

[12] Al Mahmud H., Radue M. S., Chinkanjanarot S., Pisani W. A., Gowtham S., Odegard G. M.: Multiscale modeling of carbon fiber-graphene nanoplatelet-epoxy hybrid composites using a reactive force field. Composites Part B: Engineering, **172**, 628–635 (2019). https://doi.org/10.1016/j.compositesb.2019.05.035

[13] Al Mahmud H., Patil S. U., Radue M. S., Odegard G. M.: Probing the influence of surface chemical functionalization on graphene nanoplatelets-epoxy interfacial shear strength using molecular dynamics. Nanomaterials, **13**, 287 (2023). https://doi.org/10.3390/nano13020287

[14] Al Mahmud H., Radue M. S., Chinkanjanarot S., Odegard G. M.: Multiscale modeling of epoxy-based nanocomposites reinforced with functionalized and non-functionalized graphene nanoplatelets. Polymers, **13**, 1958 (2021). https://doi.org/10.3390/polym13121958

[15] Al Mahmud H., Radue M. S., Pisani W. A., Odegard G. M.: Computational modeling of hybrid carbon fiber/epoxy composites reinforced with functionalized and non-functionalized graphene nanoplatelets. Nanomaterials, **11**, 2919 (2021). https://doi.org/10.3390/nano11112919

[16] Al Mahmud H., Radue M., Chinkanjanarot S., Pisani W., Gowtham S., Odegard G.: Predicting the effective mechanical properties of graphene nanoplatelet-carbon fiber-epoxy hybrid composites using reaxff: A multiscale modeling. in '16th Biennial International Conference on Engineering, Science, Construction, and Operations in Challenging Environments. Cleveland, USA' 556–569 (2018).

[17] Al Mahmud H., Radue M. S., Odegard G. M.: Molecular dynamics modeling to probe the effect of surface functionalization on the interfacial adhesion and shear strength of graphene/epoxy nanocomposites. in 'Earth and Space 2021. Virtual Conference, USA' 1–12 (2021).

[18] Liu L., Zhang J., Zhao J., Liu F.: Mechanical properties of graphene oxides. Nanoscale, **4**, 5910–5916 (2012). https://doi.org/10.1039/C2NR31164J

[19] Plimpton S.: Fast parallel algorithms for short-range molecular dynamics. Journal of Computational Physics, **117**, 1–19 (1995). https://doi.org/10.1006/jcph.1995.1039

[20] Jorgensen W. L., Maxwell D. S., Tirado-Rives J.: Development and testing of the opls all-atom force field on conformational energetics and properties of organic liquids. Journal of the American Chemical Society, **118**, 11225–11236 (1996). https://doi.org/10.1021/ja9621760

[21] Liu L., Liu Y., Zybin S. V., Sun H., Goddard III W. A.: ReaxFF-lg: Correction of the reaxff reactive force field for london dispersion, with applications to the equations of state for energetic materials. The Journal of Physical Chemistry A, **115**, 11016–11022 (2011). https://doi.org/10.1021/jp201599t

[22] Radue M., Odegard G. M.: Multiscale modeling of carbon fiber/carbon nanotube/epoxy hybrid composites: Comparison of epoxy matrices. Composites Science and Technology, **166**, 20–26 (2018). https://doi.org/10.1016/j.compscitech.2018.03.006

[23] Deshpande P. P., Radue M. S., Gaikwad P., Bamane S., Patil S. U., Pisani W. A., Odegard G. M.: Prediction of the interfacial properties of high-performance polymers and flattened CNT-reinforced composites using molecular dynamics. Langmuir, **37**, 11526–11534 (2021). https://doi.org/10.1021/acs.langmuir.1c01800

[24] Patil S. U., Radue M. S., Pisani W. A., Deshpande P., Xu H., Al Mahmud H., Dumitrică T., Odegard G. M.: Interfacial characteristics between flattened cnt stacks and polyimides: A molecular dynamics study. Computational Materials Science, **185**, 109970 (2020). https://doi.org/10.1016/j.commatsci.2020.109970

[25] Pisani W. A., Radue M. S., Patil S. U., Odegard G. M.: Interfacial modeling of flattened CNT composites with cyanate ester and peek polymers. Composites Part B: Engineering, **211**, 108672 (2021). https://doi.org/10.1016/j.compositesb.2021.108672

[26] Shen B., Zhai W., Chen C., Lu D., Wang J., Zheng W.: Melt blending *in situ* enhances the interaction between polystyrene and graphene through π–π stacking. ACS Applied Materials and Interfaces, **3**, 3103–3109 (2011). https://doi.org/10.1021/am200612z

[27] Zaman I., Phan T. T., Kuan H-C., Meng Q., La L. T. B., Luong L., Youssf O., Ma J.: Epoxy/graphene platelets nanocomposites with two levels of interface strength. Polymer, **52**, 1603–1611 (2011). https://doi.org/10.1016/j.polymer.2011.02.003

[28] Lv C., Xue Q., Xia D., Ma M., Xie J., Chen H.: Effect of chemisorption on the interfacial bonding characteristics of graphene–Polymer composites. The Journal of Physical Chemistry C, **114**, 6588–6594 (2010). https://doi.org/10.1021/jp100110n

[29] Lv C., Xue Q., Xia D., Ma M.: Effect of chemisorption structure on the interfacial bonding characteristics of graphene–polymer composites. Applied Surface Science, **258**, 2077–2082 (2012). https://doi.org/10.1016/j.apsusc.2011.04.056

[30] Prokhorov Y., Luna-Barcenas G., Kovalenko Y.: Interphase percolation phenomena in chitosan-graphene oxide nanocomposites, the role of water content. Express Polymer Letters, **17**, 29–39 (2023). https://doi.org/10.3144/expresspolymlett.2023.3

[31] Littell J. D., Ruggeri C. R., Goldberg R. K., Roberts G. D., Arnold W. A., Binienda W. K.: Measurement of epoxy resin tension, compression, and shear stress–strain curves over a wide range of strain rates using small test specimens. Journal of Aerospace Engineering, **21**, 162–173 (2008). https://doi.org/10.1061/(ASCE)0893-1321(2008)21:3(162)